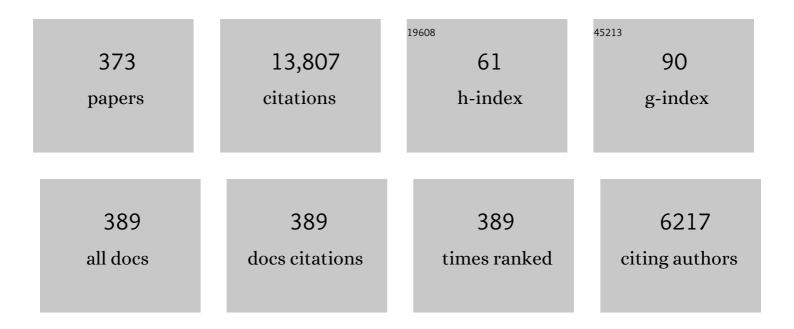
List of Publications by Year in descending order

Source: https://exaly.com/author-pdf/2305325/publications.pdf Version: 2024-02-01



Снаясьниц

#	Article	IF	CITATIONS
1	Oxidation behavior and interface diffusion of porous metal supported SOFCs with all plasma sprayed functional layers in air at 650oC. International Journal of Green Energy, 2022, 19, 818-826.	2.1	4
2	Recent advancements, doping strategies and the future perspective of perovskite-based solid oxide fuel cells for energy conversion. Chemical Engineering Journal, 2022, 428, 132603.	6.6	82
3	Recent progress of perovskite-based electrolyte materials for solid oxide fuel cells and performance optimizing strategies for energy storage applications. Materials Research Bulletin, 2022, 146, 111612.	2.7	74
4	Microstructure and Ablation Behavior of Low-Pressure Plasma Sprayed ZrB2 Coatings Down to 100 Pa. Journal of Thermal Spray Technology, 2022, 31, 282-296.	1.6	1
5	Plasma-Sprayed (Bi2O3)0.705 (Er2O3)0.245 (WO3)0.05 Electrolyte for Intermediate-Temperature Solid Oxide Fuel Cells (IT-SOFCs). Journal of Thermal Spray Technology, 2022, 31, 297-306.	1.6	4
6	Recent Research Advances in Plasma Spraying of Bulk-Like Dense Metal Coatings with Metallurgically Bonded Lamellae. Journal of Thermal Spray Technology, 2022, 31, 5-27.	1.6	15
7	Sintering behavior of BaCe0.7Zr0.1Y0.2O3-δ electrolyte at 1150°C with the utilization of CuO and Bi2O3 as sintering aids and its electrical performance. International Journal of Hydrogen Energy, 2022, 47, 7403-7414.	3.8	39
8	Critical scale grain size for optimal lifetime of TBCs. Journal of Materials Science and Technology, 2022, 115, 241-250.	5.6	12
9	Achieving high anti-sintering performance of plasma-sprayed YSZ thermal barrier coatings through pore structure design. Surface and Coatings Technology, 2022, 435, 128259.	2.2	19
10	The Bonding Formation during Thermal Spraying of Ceramic Coatings: A Review. Journal of Thermal Spray Technology, 2022, 31, 780-817.	1.6	20
11	Li3PO4 electrolyte of high conductivity for all-solid-state lithium battery prepared by plasma spray. Journal of the European Ceramic Society, 2022, 42, 4239-4247.	2.8	3
12	Thermally sprayed MCO/FeCr24 interconnector with improved stability for tubular segmented-in-series SOFCs. Applied Surface Science, 2022, 587, 152861.	3.1	7
13	Progress in ceramic materials and structure design toward advanced thermal barrier coatings. Journal of Advanced Ceramics, 2022, 11, 985-1068.	8.9	135
14	Narrow and Thin Copper Linear Pattern Deposited by Vacuum Cold Spraying and Deposition Behavior Simulation. Journal of Thermal Spray Technology, 2021, 30, 571-583.	1.6	10
15	Lightweight epoxy-based abradable seal coating with high bonding strength. Journal of Materials Science and Technology, 2021, 69, 129-137.	5.6	14
16	Dynamic evolution of oxide scale on the surfaces of feed stock particles from cracking and segmenting to peel-off while cold spraying copper powder having a high oxygen content. Journal of Materials Science and Technology, 2021, 67, 105-115.	5.6	23
17	Improving deposition efficiency and inter-particle bonding of cold sprayed Cu through removing the surficial oxide scale of the feedstock powder. Surface and Coatings Technology, 2021, 407, 126709.	2.2	13
18	Enhanced Corrosion Resistance of a Double Ceramic Composite Coating Deposited by a Novel Method on Magnesium-Lithium Alloy (LA43M) Substrates. Journal of Thermal Spray Technology, 2021, 30, 680-693.	1.6	1

#	Article	IF	CITATIONS
19	Plasma-Sprayed High-Performance (Bi2O3)0.75(Y2O3)0.25 Electrolyte for Intermediate-Temperature Solid Oxide Fuel Cells (IT-SOFCs). Journal of Thermal Spray Technology, 2021, 30, 196-204.	1.6	11
20	Effect of Powder Particle Size and Spray Parameters on the Ni/Al Reaction During Plasma Spraying of Ni-Al Composite Powders. Journal of Thermal Spray Technology, 2021, 30, 181-195.	1.6	11
21	Highly active and novel A-site deficient symmetric electrode material (Sr0.3La0.7)1â^'x (Fe0.7Ti0.3)0.9Ni0.1O3â^'δ and its effect on electrochemical performance of SOFCs. International Journal of Hydrogen Energy, 2021, 46, 8778-8791.	3.8	25
22	Performance and Stability of Plasma-Sprayed 10 × 10Âcm2 Self-sealing Metal-Supported Solid Oxide Fi Cells. Journal of Thermal Spray Technology, 2021, 30, 1059-1068.	uel 1.6	8
23	Cold spray (CS) deposition of a durable silver coating with high infrared reflectivity for radiation energy saving in the polysilicon CVD reactor. Surface and Coatings Technology, 2021, 409, 126841.	2.2	8
24	Effect of coating composition on the micro-galvanic dissolution behavior and antifouling performance of plasma-sprayed laminated-structured Cu Ti composite coating. Surface and Coatings Technology, 2021, 410, 126963.	2.2	6
25	Microstructural analysis of highly active cathode material La0.7Sr0.3Ti0.15Fe0.65Ni0.2O3-δ (LSTFN) by optimizing different processing parameters. Ceramics International, 2021, 47, 10893-10904.	2.3	15
26	Fabrication of Nanostructured Cadmium Selenide Thin Films for Optoelectronics Applications. Frontiers in Chemistry, 2021, 9, 661723.	1.8	9
27	Ni coatings for corrosion protection of Mg alloys prepared by an in-situ micro-forging assisted cold spray: Effect of powder feedstock characteristics. Corrosion Science, 2021, 184, 109397.	3.0	22
28	Capturing cold-spray bonding features of pure Cu from in situ deformation behavior using a high-accuracy material model. Surface and Coatings Technology, 2021, 413, 127087.	2.2	5
29	Sintering behavior and electrochemical performance of A-site deficient SrxTi0.3Fe0·7O3-δ oxygen electrodes for solid oxide electrochemical cells. Ceramics International, 2021, 47, 25051-25058.	2.3	13
30	Numerical Simulation of Plasma Jet Characteristics under Very Low-Pressure Plasma Spray Conditions. Coatings, 2021, 11, 726.	1.2	9
31	Novel long laminar plasma sprayed hybrid structure thermal barrier coatings for high-temperature anti-sintering and volcanic ash corrosion resistance. Journal of Materials Science and Technology, 2021, 79, 141-146.	5.6	6
32	Plasma-sprayed lanthanum-doped strontium titanate as an interconnect for solid oxide fuel cells: Effects of powder size and process conditions. Journal of Alloys and Compounds, 2021, 876, 160212.	2.8	6
33	Numerical Analysis of the Interactions between Plasma Jet and Powder Particles in PS-PVD Conditions. Coatings, 2021, 11, 1154.	1.2	0
34	Preparation of bulk-like La0.8Sr0.2Ga0.8Mg0.2O3-δ coatings for porous metal-supported solid oxide fuel cells via plasma spraying at increased particle temperatures. International Journal of Hydrogen Energy, 2021, 46, 32655-32664.	3.8	8
35	TGO and Al diffusion behavior of CuAlxNiCrFe high-entropy alloys fabricated by high-speed laser cladding for TBC bond coats. Corrosion Science, 2021, 192, 109781.	3.0	21
36	In-situ heating effect of laminar plasma jet during Mo coatings deposition. Materials Letters, 2021, 305, 130743.	1.3	1

#	Article	IF	CITATIONS
37	Enhancement of Corrosion Resistance and Tribological Properties of LA43M Mg Alloy by Cold-Sprayed Aluminum Coatings Reinforced with Alumina and Carbon Nanotubes. Journal of Thermal Spray Technology, 2021, 30, 668-679.	1.6	10
38	Enhancing the hot-corrosion resistance of atmospheric plasma sprayed Ni-based coatings by adding a deoxidizer. Materials and Design, 2021, 211, 110154.	3.3	12
39	Towards better understanding supersonic impact-bonding behavior of cold sprayed 6061-T6 aluminum alloy based on a high-accuracy material model. Additive Manufacturing, 2021, 48, 102469.	1.7	2
40	Large-grain \hat{l} ±-Al2O3 enabling ultra-high oxidation-resistant MCrAlY bond coats by surface pre-agglomeration treatment. Corrosion Science, 2020, 163, 108275.	3.0	31
41	Dense Mn1.5Co1.5O4 coatings with excellent long-term stability and electrical performance under the SOFC cathode environment. Applied Surface Science, 2020, 499, 143726.	3.1	37
42	Improving WC-Co coating adhesive strength on rough substrate: Finite element modeling and experiment. Journal of Materials Science and Technology, 2020, 37, 1-8.	5.6	16
43	A Novel Strategy for Depositing Dense Self-fluxing Alloy Coatings with Sufficiently Bonded Splats by One-Step Atmospheric Plasma Spraying. Journal of Thermal Spray Technology, 2020, 29, 173-184.	1.6	15
44	Effects of Powder Structure and Size on Gd2O3 Preferential Vaporization During Plasma Spraying of Gd2Zr2O7. Journal of Thermal Spray Technology, 2020, 29, 105-114.	1.6	5
45	Improving adhesive strength of WC-CoCr coating with novel bimodal roughening substrate: Finite element modeling. Ceramics International, 2020, 46, 10481-10489.	2.3	0
46	Morphology of composite coatings formed on Mo1 substrate using hot-dip aluminising and micro-arc oxidation techniques. Applied Surface Science, 2020, 508, 144761.	3.1	10
47	Effect of water environment on particle deposition of underwater cold spray. Applied Surface Science, 2020, 506, 144542.	3.1	17
48	Optimization of Plasma-Sprayed Lanthanum Chromite Interconnector Through Powder Design and Critical Process Parameters Control. Journal of Thermal Spray Technology, 2020, 29, 212-222.	1.6	12
49	Development of ScSZ Electrolyte by Very Low Pressure Plasma Spraying for High-Performance Metal-Supported SOFCs. Journal of Thermal Spray Technology, 2020, 29, 223-231.	1.6	17
50	Plasma-Sprayed Al Alloy Coating with Enhanced Lamellar Bonding Through Novel Self-Bonding Strategy. Jom, 2020, 72, 4604-4612.	0.9	2
51	Self-Sealing Metal-Supported SOFC Fabricated by Plasma Spraying and Its Performance under Unbalanced Gas Pressure. Journal of Thermal Spray Technology, 2020, 29, 2001-2011.	1.6	10
52	High performance of ceramic current collector fabricated at 550°C through in-situ joining of reduced Mn1.5Co1.5O4 for metal-supported solid oxide fuel cells. International Journal of Hydrogen Energy, 2020, 45, 29123-29130.	3.8	7
53	Deposition and oxidation behavior of atmospheric laminar plasma sprayed Mo coatings from 200Âmm to 400Âmm under 20ÂkW: Numerical and experimental analyses. Surface and Coatings Technology, 2020, 400, 126245.	2.2	9
54	Study on Deposition Behavior of Less Than 5Âμm YSZ Particles in VLPPS. Journal of Thermal Spray Technology, 2020, 29, 1708-1717.	1.6	3

#	Article	IF	CITATIONS
55	Advanced oxygen-electrode-supported solid oxide electrochemical cells with Sr(Ti,Fe)O _{3â^îÎ} -based fuel electrodes for electricity generation and hydrogen production. Journal of Materials Chemistry A, 2020, 8, 25867-25879.	5.2	16
56	Fabrication of Metal Matrix Composites via High-Speed Particle Implantation. Journal of Thermal Spray Technology, 2020, 29, 1910-1925.	1.6	1
57	Self-Bonding Effect Development for Plasma Spraying of Stainless Steel Coating Through Using Mo-Clad Stainless Steel Powders. Jom, 2020, 72, 4613-4623.	0.9	3
58	Splash involved deposition behavior and erosion mechanism of long laminar plasma sprayed NiCrBSi coatings. Surface and Coatings Technology, 2020, 395, 125939.	2.2	8
59	Enhanced corrosion resistance of cold-sprayed and shot-peened aluminum coatings on LA43M magnesium alloy. Surface and Coatings Technology, 2020, 394, 125865.	2.2	50
60	High-temperature oxidation behavior of CuAlNiCrFe high-entropy alloy bond coats deposited using high-speed laser cladding process. Surface and Coatings Technology, 2020, 398, 126093.	2.2	60
61	Performance evaluation of highly active and novel La0.7Sr0.3Ti0.1Fe0.6Ni0.3O3-δ material both as cathode and anode for intermediate-temperature symmetrical solid oxide fuel cell. Journal of Power Sources, 2020, 472, 228498.	4.0	54
62	Numerical analysis of the plasma-induced self-shadowing effect of impinging particles and phase transformation in a novel long laminar plasma jet. Journal Physics D: Applied Physics, 2020, 53, 375202.	1.3	11
63	Plasma spray–physical vapor deposition toward advanced thermal barrier coatings: a review. Rare Metals, 2020, 39, 479-497.	3.6	33
64	Microstructures of aluminum surfaces reinforced with 316L stainless steel particles via high-speed particle injection and the resulting double-strengthening mechanism. Surface and Coatings Technology, 2020, 385, 125380.	2.2	6
65	Solid-state additive manufacturing high performance aluminum alloy 6061 enabled by an in-situ micro-forging assisted cold spray. Materials Science & Engineering A: Structural Materials: Properties, Microstructure and Processing, 2020, 776, 139024.	2.6	44
66	Structured La0.6Sr0.4Co0.2Fe0.8O3-ĺ′ cathode with large-scale vertical cracks by atmospheric laminar plasma spraying for IT-SOFCs. Journal of Alloys and Compounds, 2020, 825, 153865.	2.8	18
67	Superior oxidation resistant MCrAlY bond coats prepared by controlled atmosphere heat treatment. Corrosion Science, 2020, 170, 108653.	3.0	39
68	Bioinspired Mechanically Robust Metalâ€Based Water Repellent Surface Enabled by Scalable Construction of a Flexible Coralâ€Reefâ€Like Architecture. Small, 2019, 15, e1901919.	5.2	30
69	Deposition of fully dense Al-based coatings via in-situ micro-forging assisted cold spray for excellent corrosion protection of AZ31B magnesium alloy. Journal of Alloys and Compounds, 2019, 806, 1116-1126.	2.8	66
70	High stability SrTi _{1â^'x} Fe _x O _{3â^'î} electrodes for oxygen reduction and oxygen evolution reactions. Journal of Materials Chemistry A, 2019, 7, 21447-21458.	5.2	32
71	The Characteristics of Cermet-Supported Tubular Solid Oxide Fuel Cells Manufactured by Thermal Spraying. ECS Transactions, 2019, 91, 285-289.	0.3	2
72	Characterization of Self-Sealed Metal Supported SOFCs with the Very Low Pressure Plasma Sprayed ScSZ Electrolyte. ECS Transactions, 2019, 91, 901-908.	0.3	2

#	Article	IF	CITATIONS
73	Transport and deposition behaviors of vapor coating materials in plasma spray-physical vapor deposition. Applied Surface Science, 2019, 486, 80-92.	3.1	60
74	Numerical simulation of the flow characteristics inside a novel plasma spray torch. Journal Physics D: Applied Physics, 2019, 52, 335203.	1.3	27
75	Electrochemical performance and stability of SrTi0.3Fe0.6Co0.1O3-δ infiltrated La0.8Sr0.2MnO3Zr0.92Y0.16O2-δ oxygen electrodes for intermediate-temperature solid oxide electrochemical cells. Journal of Power Sources, 2019, 426, 233-241.	4.0	27
76	Highly oxidation resistant MCrAlY bond coats prepared by heat treatment under low oxygen content. Surface and Coatings Technology, 2019, 368, 192-201.	2.2	66
77	Effect of substrate temperature on the microstructure and interface bonding formation of plasma sprayed Ni20Cr splat. Surface and Coatings Technology, 2019, 371, 36-46.	2.2	14
78	Microstructural evolution of alumina coatings by a novel long laminar plasma spraying method. Surface and Coatings Technology, 2019, 363, 210-220.	2.2	12
79	Combined effect of internal and external factors on sintering kinetics of plasma-sprayed thermal barrier coatings. Journal of the European Ceramic Society, 2019, 39, 1860-1868.	2.8	37
80	Thermodynamic conditions for cluster formation in supersaturated boundary layer during plasma spray-physical vapor deposition. Applied Surface Science, 2019, 471, 950-959.	3.1	49
81	Plasma Spraying of Dense Ceramic Coating with Fully Bonded Lamellae Through Materials Design Based on the Critical Bonding Temperature Concept. Journal of Thermal Spray Technology, 2019, 28, 53-62.	1.6	15
82	Highly stable carbon-based perovskite solar cell with a record efficiency of over 18% via hole transport engineering. Journal of Materials Science and Technology, 2019, 35, 987-993.	5.6	123
83	Generation of Long Laminar Plasma Jets: Experimental and Numerical Analyses. Plasma Chemistry and Plasma Processing, 2019, 39, 377-394.	1.1	20
84	Visible light enhanced black NiO sensors for ppb-level NO2 detection at room temperature. Ceramics International, 2019, 45, 4253-4261.	2.3	63
85	Molecular dynamics simulation and experimental verification for bonding formation of solid-state TiO2 nano-particles induced by high velocity collision. Ceramics International, 2019, 45, 4700-4706.	2.3	7
86	Cracking induced tribological behavior changes for the HVOF WC-12Co cermet coatings. Ceramics International, 2019, 45, 4718-4728.	2.3	19
87	Corrosion resistant nickel coating with strong adhesion on AZ31B magnesium alloy prepared by an in-situ shot-peening-assisted cold spray. Corrosion Science, 2018, 138, 105-115.	3.0	123
88	Vacuum heat treatment mechanisms promoting the adhesion strength of thermally sprayed metallic coatings. Surface and Coatings Technology, 2018, 344, 102-110.	2.2	52
89	Cost effective perovskite solar cells with a high efficiency and open-circuit voltage based on a perovskite-friendly carbon electrode. Journal of Materials Chemistry A, 2018, 6, 8271-8279.	5.2	57
90	Substrate-constrained effect on the stiffening behavior of lamellar thermal barrier coatings. Journal of the European Ceramic Society, 2018, 38, 2579-2587.	2.8	14

#	Article	IF	CITATIONS
91	Sodium ionic conductivity and stability of amorphous Na 2 O·2SiO 2 added with M x O y (M = Zr, Y, and) Tj ETQo	1 <u>1</u> 10.784ع	4314 rgBT (
92	Microstructure and Transparent Super-Hydrophobic Performance of Vacuum Cold-Sprayed Al2O3 and SiO2 Aerogel Composite Coating. Journal of Thermal Spray Technology, 2018, 27, 471-482.	1.6	15
93	Achieving the high phase purity of CH3NH3PbI3 film by two-step solution processable crystal engineering. Journal of Materials Science and Technology, 2018, 34, 1405-1411.	5.6	12
94	The Effect of Molybdenum Substrate Oxidation on Molybdenum Splat Formation. Journal of Thermal Spray Technology, 2018, 27, 14-24.	1.6	9
95	Development of long laminar plasma jet on thermal spraying process: Microstructures of zirconia coatings. Surface and Coatings Technology, 2018, 337, 241-249.	2.2	22
96	Highly oxidation resistant and cost effective MCrAlY bond coats prepared by controlled atmosphere heat treatment. Surface and Coatings Technology, 2018, 347, 54-65.	2.2	76
97	Novel Method of Aluminum to Copper Bonding by Cold Spray. Journal of Thermal Spray Technology, 2018, 27, 624-640.	1.6	23
98	Stage-sensitive microstructural evolution of nanostructured TBCs during thermal exposure. Journal of the European Ceramic Society, 2018, 38, 3325-3332.	2.8	32
99	Low-temperature SnO ₂ -modified TiO ₂ yields record efficiency for normal planar perovskite solar modules. Journal of Materials Chemistry A, 2018, 6, 10233-10242.	5.2	75
100	Gaseous material capacity of open plasma jet in plasma spray-physical vapor deposition process. Applied Surface Science, 2018, 428, 877-884.	3.1	49
101	Improving Erosion Resistance of Plasma-Sprayed Ceramic Coatings by Elevating the Deposition Temperature Based on the Critical Bonding Temperature. Journal of Thermal Spray Technology, 2018, 27, 25-34.	1.6	5
102	Effect of the shell-core-structured particle design on the heating characteristic of nickel-based alloy particle during plasma spraying. Surface and Coatings Technology, 2018, 335, 52-61.	2.2	13
103	Tailoring the composite interface at lower temperature by the nanoscale interfacial active layer formed in cold sprayed cBN/NiCrAl nanocomposite. Materials and Design, 2018, 140, 387-399.	3.3	14
104	A new approach to prepare fully dense Cu with high conductivities and anti-corrosion performance by cold spray. Journal of Alloys and Compounds, 2018, 740, 406-413.	2.8	40
105	Sintering characteristics of plasma-sprayed TBCs: Experimental analysis and an overall modelling. Ceramics International, 2018, 44, 2982-2990.	2.3	44
106	Effect of Post-spray Shot Peening Treatment on the Corrosion Behavior of NiCr-Mo Coating by Plasma Spraying of the Shell–Core–Structured Powders. Journal of Thermal Spray Technology, 2018, 27, 232-242.	1.6	17
107	Gradient thermal cyclic behaviour of La2Zr2O7/YSZ DCL-TBCs with equivalent thermal insulation performance. Journal of the European Ceramic Society, 2018, 38, 1888-1896.	2.8	57
108	Effect of vapor deposition in shrouded plasma spraying on morphology and wettability of the metallic Ni20Cr coating surface. Journal of Alloys and Compounds, 2018, 735, 430-440.	2.8	19

#	Article	IF	CITATIONS
109	Mechanical performance of plasma-sprayed bulk-like NiCrMo coating with a novel shell-core-structured NiCr-Mo particle. Surface and Coatings Technology, 2018, 353, 179-189.	2.2	14
110	Comprehensive dynamic failure mechanism of thermal barrier coatings based on a novel crack propagation and TGO growth coupling model. Ceramics International, 2018, 44, 22556-22566.	2.3	56
111	Performance of La0.8Sr0.2Ga0.8Mg0.2O3-based SOFCs with atmospheric plasma sprayed La-doped CeO2 buffer layer. Electrochimica Acta, 2018, 275, 208-217.	2.6	15
112	A novel structure of YSZ coatings by atmospheric laminar plasma spraying technology. Scripta Materialia, 2018, 153, 73-76.	2.6	41
113	La0.8Sr0.2Ga0.8Mg0.2O3 electrolytes prepared by vacuum cold spray under heated gas for improved performance of SOFCs. Ceramics International, 2018, 44, 13773-13781.	2.3	9
114	Strain/sintering co-induced multiscale structural changes in plasma-sprayed thermal barrier coatings. Ceramics International, 2018, 44, 14408-14416.	2.3	23
115	Cobalt-substituted SrTi _{0.3} Fe _{0.7} O _{3â^î^} : a stable high-performance oxygen electrode material for intermediate-temperature solid oxide electrochemical cells. Energy and Environmental Science, 2018, 11, 1870-1879.	15.6	93
116	Prolong the durability of La2Zr2O7/YSZ TBCs by decreasing the cracking driving force in ceramic coatings. Journal of the European Ceramic Society, 2018, 38, 5482-5488.	2.8	51
117	MD Simulation on Collision Behavior Between Nano-Scale TiO ₂ Particles During Vacuum Cold Spraying. Journal of Nanoscience and Nanotechnology, 2018, 18, 2657-2664.	0.9	5
118	Deposition behavior, microstructure and mechanical properties of an in-situ micro-forging assisted cold spray enabled additively manufactured Inconel 718 alloy. Materials and Design, 2018, 155, 384-395.	3.3	64
119	Effect of the powder particle structure and substrate hardness during vacuum cold spraying of Al 2 O 3. Ceramics International, 2017, 43, 4390-4398.	2.3	34
120	Strain-induced multiscale structural changes in lamellar thermal barrier coatings. Ceramics International, 2017, 43, 2252-2266.	2.3	35
121	Sinteringâ€induced delamination of thermal barrier coatings by gradient thermal cyclic test. Journal of the American Ceramic Society, 2017, 100, 1820-1830.	1.9	74
122	Material nucleation/growth competition tuning towards highly reproducible planar perovskite solar cells with efficiency exceeding 20%. Journal of Materials Chemistry A, 2017, 5, 6840-6848.	5.2	149
123	Ultra-high open-circuit voltage of perovskite solar cells induced by nucleation thermodynamics on rough substrates. Scientific Reports, 2017, 7, 46141.	1.6	71
124	A comprehensive mechanism for the sintering of plasma-sprayed nanostructured thermal barrier coatings. Ceramics International, 2017, 43, 9600-9615.	2.3	60
125	Thermally Sprayed Large Tubular Solid Oxide Fuel Cells and Its Stack: Geometry Optimization, Preparation, and Performance. Journal of Thermal Spray Technology, 2017, 26, 441-455.	1.6	16
126	Influence of microstructure on the mechanical integrity of plasma-sprayed TiO2 splat. Journal of the European Ceramic Society, 2017, 37, 4979-4989.	2.8	5

#	Article	IF	CITATIONS
127	Edge Effect on Crack Patterns in Thermally Sprayed Ceramic Splats. Journal of Thermal Spray Technology, 2017, 26, 302-314.	1.6	34
128	Effect of Fe doping on the performance of suspension plasma-sprayed PrBa0.5Sr0.5Co2â^'xFexO5+δ cathodes for intermediate-temperature solid oxide fuel cells. Ceramics International, 2017, 43, 11648-11655.	2.3	26
129	Super-Hydrophobic Surface Prepared by Lanthanide Oxide Ceramic Deposition Through PS-PVD Process. Journal of Thermal Spray Technology, 2017, 26, 398-408.	1.6	11
130	Epitaxial growth during the rapid solidification of plasma-sprayed molten TiO 2 splat. Acta Materialia, 2017, 134, 66-80.	3.8	33
131	Force transmission and its effect on structural changes in plasma-sprayed lamellar ceramic coatings. Journal of the European Ceramic Society, 2017, 37, 2877-2888.	2.8	30
132	Non-parabolic isothermal oxidation kinetics of low pressure plasma sprayed MCrAlY bond coat. Applied Surface Science, 2017, 406, 99-109.	3.1	69
133	Large-area high-efficiency perovskite solar cells based on perovskite films dried by the multi-flow air knife method in air. Journal of Materials Chemistry A, 2017, 5, 1548-1557.	5.2	115
134	Effect of Oxidation on the Bonding Formation of Plasma-Sprayed Stainless Steel Splats onto Stainless Steel Substrate. Journal of Thermal Spray Technology, 2017, 26, 47-59.	1.6	14
135	Optimization of In-Situ Shot-Peening-Assisted Cold Spraying Parameters for Full Corrosion Protection of Mg Alloy by Fully Dense Al-Based Alloy Coating. Journal of Thermal Spray Technology, 2017, 26, 173-183.	1.6	65
136	Influence of pre-reduction on microstructure homogeneity and electrical properties of APS Mn1.5Co1.5O4 coatings for SOFC interconnects. International Journal of Hydrogen Energy, 2017, 42, 27241-27253.	3.8	28
137	Sintering induced the failure behavior of dense vertically crack and lamellar structured TBCs with equivalent thermal insulation performance. Ceramics International, 2017, 43, 15459-15465.	2.3	62
138	Fast Drying Boosted Performance Improvement of Low-Temperature Paintable Carbon-Based Perovskite Solar Cell. ACS Sustainable Chemistry and Engineering, 2017, 5, 9758-9765.	3.2	35
139	Microstructure and Electrochemical Properties of La0.8Sr0.2Ga0.8Mg0.2O3Thin Film Deposited by Vacuum Cold Spray for Solid Oxide Fuel Cells. ECS Transactions, 2017, 78, 405-412.	0.3	3
140	Atmospheric Plasma-Sprayed La0.3Sr0.7TiO3-Î1nterconnect for High-Temperature Solid Oxide Fuel Cells. ECS Transactions, 2017, 78, 1653-1663.	0.3	1
141	Novel Approaches to Prepare the High Performance Dense Electolyte and Interconnect Applicable to SOFC by Atmospheric Plasma Spraying. ECS Transactions, 2017, 78, 1831-1838.	0.3	2
142	Study on the Fabrication and Performance of Very Low Pressure Plasma Sprayed Porous Metal Supported Solid Oxide Fuel Cell. ECS Transactions, 2017, 78, 2059-2067.	0.3	4
143	Effect of Deposition Temperature on the Microstructure and Performance of Vacuum Cold Sprayed Nano-Structured LSCF Cathodes for Solid Oxide Fuel Cells. ECS Transactions, 2017, 78, 765-772.	0.3	1
144	Small molecule-driven directional movement enabling pin-hole free perovskite film via fast solution engineering. Nanoscale, 2017, 9, 15778-15785.	2.8	2

#	Article	IF	CITATIONS
145	Evaporation of Droplets in Plasma Spray–Physical Vapor Deposition Based on Energy Compensation Between Self-Cooling and Plasma Heat Transfer. Journal of Thermal Spray Technology, 2017, 26, 1641-1650.	1.6	24
146	The Correlation of the TBC Lifetimes in Burner Cycling Test with Thermal Gradient and Furnace Isothermal Cycling Test by TGO Effects. Journal of Thermal Spray Technology, 2017, 26, 378-387.	1.6	50
147	Enhanced sintering behavior of LSGM electrolyte and its performance for solid oxide fuel cells deposited by vacuum cold spray. Journal of the European Ceramic Society, 2017, 37, 4751-4761.	2.8	15
148	Suspension Plasma Sprayed Sr2Fe1.4Mo0.6O6â~δElectrodes for Solid Oxide Fuel Cells. Journal of Thermal Spray Technology, 2017, 26, 432-440.	1.6	2
149	Room-temperature nitrogen-dioxide sensors based on ZnO1â^'x coatings deposited by solution precursor plasma spray. Sensors and Actuators B: Chemical, 2017, 242, 102-111.	4.0	65
150	Dependence of scale thickness on the breaking behavior of the initial oxide on plasma spray bond coat surface during vacuum pre-treatment. Applied Surface Science, 2017, 397, 125-132.	3.1	33
151	Dominant effect of particle size on the CeO2 preferential evaporation during plasma spraying of La2Ce2O7. Journal of the European Ceramic Society, 2017, 37, 1577-1585.	2.8	22
152	Dependency of deposition behavior, microstructure and properties of cold sprayed Cu on morphology and porosity of the powder. Surface and Coatings Technology, 2017, 328, 304-312.	2.2	22
153	Properties evolution of plasma-sprayed La2Zr2O7 coating induced by pore structure evolution during thermal exposure. Ceramics International, 2016, 42, 15485-15492.	2.3	41
154	The 2016 Thermal Spray Roadmap. Journal of Thermal Spray Technology, 2016, 25, 1376-1440.	1.6	243
155	The Microstructure Stability of Atmospheric Plasma-Sprayed MnCo2O4 Coating Under Dual-Atmosphere (H2/Air) Exposure. Journal of Thermal Spray Technology, 2016, 25, 301-310.	1.6	5
156	La2NiO4+δ Infiltration of Plasma-Sprayed LSCF Coating for Cathode Performance Improvement. Journal of Thermal Spray Technology, 2016, 25, 392-400.	1.6	15
157	Formation of Cr2O3 Diffusion Barrier Between Cr-Contained Stainless Steel and Cold-Sprayed Ni Coatings at High Temperature. Journal of Thermal Spray Technology, 2016, 25, 526-534.	1.6	13
158	Investigation into the diffusion and oxidation behavior of the interface between a plasma-sprayed anode and a porous steel support for solid oxide fuel cells. Journal of Power Sources, 2016, 323, 1-7.	4.0	5
159	<i>In Situ</i> Formation of Continuous Charge Transfer Pathways for Highly Efficient, Solvent-Free, Polymer Electrolyte-Based Dye-Sensitized Solar Cells. ACS Sustainable Chemistry and Engineering, 2016, 4, 4013-4020.	3.2	8
160	Thermally sprayed high-performance porous metal-supported solid oxide fuel cells with nanostructured La _{0.6} Sr _{0.4} Co _{0.2} Fe _{0.8} O _{3â^Î} cathodes. Journal of Materials Chemistry A, 2016, 4, 7461-7468.	5.2	25
161	Realizing full coverage of perovskite film on substrate surface during solution processing: Characterization and elimination of uncovered surface. Journal of Power Sources, 2016, 320, 204-211.	4.0	18
162	Aerosol sprayed Mn 1.5 Co 1.5 O 4 protective coatings for metallic interconnect of solid oxide fuel cells. International Journal of Hydrogen Energy, 2016, 41, 20305-20313.	3.8	11

#	Article	IF	CITATIONS
163	Formation of Al2O3 diffusion barrier in cold-sprayed NiCoCrAlY/Ni multi-layered coatings on 304SS substrate. Surface and Coatings Technology, 2016, 307, 603-609.	2.2	13
164	Nonâ€destructive production of natural environmentâ€adaptive superâ€hydrophobic hierarchical ceramic surface on a steel substrate. Micro and Nano Letters, 2016, 11, 680-683.	0.6	2
165	Conditions and mechanisms for the bonding of a molten ceramic droplet to a substrate after high-speed impact. Acta Materialia, 2016, 119, 9-25.	3.8	67
166	Liquid plasma sprayed nano-network La0.4Sr0.6Co0.2Fe0.8O3/Ce0.8Gd0.2O2 composite as a high-performance cathode for intermediate-temperature solid oxide fuel cells. Journal of Power Sources, 2016, 327, 622-628.	4.0	7
167	Relationship Between Designed Three-Dimensional YSZ Electrolyte Surface Area and Performance of Solution-Precursor Plasma-Sprayed La0.8Sr0.2MnO3â^Î Cathodes. Journal of Thermal Spray Technology, 2016, 25, 1692-1699.	1.6	2
168	Understanding the Formation of Limited Interlamellar Bonding in PlasmaÂSprayed Ceramic Coatings Based on the Concept of Intrinsic Bonding Temperature. Journal of Thermal Spray Technology, 2016, 25, 1617-1630.	1.6	22
169	Preparation of hierarchical porous metallic materials via deposition of microporous particles. Materials Letters, 2016, 176, 237-240.	1.3	8
170	Hierarchical Formation of Intrasplat Cracks in Thermal Spray Ceramic Coatings. Journal of Thermal Spray Technology, 2016, 25, 959-970.	1.6	41
171	Influence of TiO ₂ Film/Substrate Contact on Photovoltaic Performance and Improved Efficiency in Dye-Sensitized Solar Cells. Journal of Nanoscience and Nanotechnology, 2016, 16, 7395-7403.	0.9	1
172	Microstructure of YSZ Coatings Deposited by PS-PVD Using 45ÂkW Shrouded Plasma Torch. Materials and Manufacturing Processes, 2016, 31, 1183-1191.	2.7	18
173	Plasma-Sprayed Thermal Barrier Coatings with Enhanced Splat Bonding for CMAS and Corrosion Protection. Journal of Thermal Spray Technology, 2016, 25, 213-221.	1.6	31
174	An effective approach for creating metallurgical self-bonding in plasma-spraying of NiCr-Mo coating by designing shell-core-structured powders. Acta Materialia, 2016, 110, 19-30.	3.8	90
175	Microstructure and Properties of Porous Abradable Alumina Coatings Flame-Sprayed with Semi-molten Particles. Journal of Thermal Spray Technology, 2016, 25, 264-272.	1.6	13
176	Effect of spray conditions on deposition behavior and microstructure of cold sprayed Ni coatings sprayed with a porous electrolytic Ni powder. Surface and Coatings Technology, 2016, 289, 85-93.	2.2	49
177	Preparation of flexible perovskite solar cells by a gas pump drying method on a plastic substrate. Journal of Materials Chemistry A, 2016, 4, 3704-3710.	5.2	87
178	High Heat Insulating Thermal Barrier Coating Designed with Large Two-Dimensional Inter-lamellar Pores. Journal of Thermal Spray Technology, 2016, 25, 222-230.	1.6	12
179	Thermal stability of plasma-sprayed La2Ce2O7/YSZ composite coating. Ceramics International, 2016, 42, 7950-7961.	2.3	16
180	Impact of deposition temperature on crystalline structure of plasma-sprayed Al2O3 splats revealed by FIB-HRTEM technique. Ceramics International, 2016, 42, 853-860.	2.3	23

#	Article	IF	CITATIONS
181	Impact-induced bonding and boundary amorphization of TiN ceramic particles during room temperature vacuum cold spray deposition. Ceramics International, 2016, 42, 1640-1647.	2.3	23
182	Application of high velocity oxygen fuel flame (HVOF) spraying toÂfabrication of La0.8Sr0.2Ga0.8Mg0.2O3 electrolyte for solid oxide fuelÂcells. Journal of Power Sources, 2016, 301, 62-71.	4.0	17
183	A comparison of cold spray deposition behavior between gas atomized and dendritic porous electrolytic Ni powders under the same spray conditions. Materials Letters, 2016, 163, 58-60.	1.3	27
184	WC-Co Composite Coating Deposited by Cold Spraying of a Core-Shell-Structured WC-Co Powder. Journal of Thermal Spray Technology, 2015, 24, 100.	1.6	13
185	Relationship Between Lamellar Structure and Elastic Modulus of Thermally Sprayed Thermal Barrier Coatings with Intra-splat Cracks. Journal of Thermal Spray Technology, 2015, 24, 1355-1367.	1.6	74
186	Mechanical property and wear performance dependence on processing condition for cold-sprayed WC-(nanoWC-Co). Applied Surface Science, 2015, 332, 80-88.	3.1	47
187	Failure mechanism for flexible dye-sensitized solar cells under repeated outward bending: Cracking and spalling off of nano-porous titanium dioxide film. Journal of Power Sources, 2015, 280, 182-189.	4.0	16
188	Ceramic Nano-particle/Substrate Interface Bonding Formation Derived from Dynamic Mechanical Force at Room Temperature: HRTEM Examination. Journal of Thermal Spray Technology, 2015, 24, 720-728.	1.6	7
189	Healing of the Interface Between Splashed Particles and Underlying Bulk Coating and Its Influence on Isothermal Oxidation Behavior of LPPS MCrAlY Bond Coat. Journal of Thermal Spray Technology, 2015, 24, 611-621.	1.6	29
190	A TEM Study of the Microstructure of Plasma-Sprayed YSZ Near Inter-splat Interfaces. Journal of Thermal Spray Technology, 2015, 24, 907-914.	1.6	16
191	Large sized cubic BN reinforced nanocomposite with improved abrasive wear resistance deposited by cold spray. Materials and Design, 2015, 83, 249-256.	3.3	46
192	Epitaxial grain growth during 8YSZ splat formation on polycrystalline YSZ substrates by plasma spraying. Surface and Coatings Technology, 2015, 274, 37-43.	2.2	24
193	The influence of temperature gradient across YSZ on thermal cyclic lifetime of plasma-sprayed thermal barrier coatings. Ceramics International, 2015, 41, 11046-11056.	2.3	55
194	Microstructure and mechanical property of Ti and Ti6Al4V prepared by an in-situ shot peening assisted cold spraying. Materials and Design, 2015, 85, 527-533.	3.3	149
195	Atmospheric plasma-sprayed La _{0.8} Sr _{0.2} Ga _{0.8} Mg _{0.2} O ₃ electrolyte membranes for intermediate-temperature solid oxide fuel cells. Journal of Materials Chemistry A, 2015, 3. 7535-7553.	5.2	50
196	Characterization of Plasma Jet in Plasma Spray-Physical Vapor Deposition of YSZ Using a <80ÂkW Shrouded Torch Based on Optical Emission Spectroscopy. Journal of Thermal Spray Technology, 2015, 24, 1038-1045.	1.6	37
197	Morphology and Size Evolution of Interlamellar Two-Dimensional Pores in Plasma-Sprayed La2Zr2O7 Coatings During Thermal Exposure at 1300°C. Journal of Thermal Spray Technology, 2015, 24, 739-748.	1.6	48
198	Unexpected efficiency enhancement of flexible dye-sensitized solar cells by repeated outward bending. RSC Advances, 2015, 5, 85174-85178.	1.7	1

#	Article	IF	CITATIONS
199	Relationships between the properties and microstructure of Mo–Cu composites prepared by infiltrating copper into flame-sprayed porous Mo skeleton. Materials and Design, 2015, 88, 774-780.	3.3	31
200	Behavioral study of flexible platinum counter electrodes under alternative bending conditions. RSC Advances, 2015, 5, 73155-73161.	1.7	1
201	Controlling grain size in columnar YSZ coating formation by droplet filtering assisted PS-PVD processing. RSC Advances, 2015, 5, 102126-102133.	1.7	11
202	Propagation feature of cracks in plasma-sprayed YSZ coatings under gradient thermal cycling. Ceramics International, 2015, 41, 3481-3489.	2.3	41
203	Fabrication of Porous Stainless Steel by Flame Spraying of Semimolten Particles. Materials and Manufacturing Processes, 2014, 29, 1253-1259.	2.7	10
204	Plasma-Sprayed Y2O3-Stabilized ZrO2 Electrolyte With Improved Interlamellar Bonding for Direct Application to Solid Oxide Fuel Cells. Journal of Fuel Cell Science and Technology, 2014, 11, .	0.8	17
205	Effect of intersplat interface bonding on the microstructure of plasma-sprayed Al2O3 coating. IOP Conference Series: Materials Science and Engineering, 2014, 61, 012022.	0.3	12
206	Nano-Porous TiO ₂ Layer Using Ultrafine Nano-Particles for the Blocking Layer in Dye-Sensitized Solar Cells. Journal of Nanoscience and Nanotechnology, 2014, 14, 2829-2835.	0.9	5
207	Splat interface bonding formation during plasma spraying of LZO coating. Materials Research Innovations, 2014, 18, S4-973-S4-978.	1.0	0
208	Room temperature cold sprayed TiO2 scattering layer for high performance and bending resistant plastic-based dye-sensitized solar cells. Journal of Power Sources, 2014, 251, 122-129.	4.0	18
209	Evolution of microstructure during annealing of Mn1.5Co1.5O4 spinel coatings deposited by atmospheric plasma spray. International Journal of Hydrogen Energy, 2014, 39, 13844-13851.	3.8	22
210	Effect of <scp><scp>TGO</scp></scp> Thickness on Thermal Cyclic Lifetime and Failure Mode of Plasma‧prayed <scp><scp>TBC</scp>s. Journal of the American Ceramic Society, 2014, 97, 1226-1232.</scp>	1.9	157
211	High velocity impact induced microstructure evolution during deposition of cold spray coatings: A review. Surface and Coatings Technology, 2014, 254, 11-20.	2.2	165
212	Microstructure, Mechanical Properties, and Two-Body Abrasive Wear Behavior of Cold-Sprayed 20Âvol.% Cubic BN-NiCrAl Nanocomposite Coating. Journal of Thermal Spray Technology, 2014, 23, 1181-1190.	1.6	14
213	Deposition Behavior of Semi-Molten Spray Particles During Flame Spraying of Porous Metal Alloy. Journal of Thermal Spray Technology, 2014, 23, 991-999.	1.6	20
214	Chemical compatibility and properties of suspension plasma-sprayed SrTiO3-based anodes for intermediate-temperature solid oxide fuel cells. Journal of Power Sources, 2014, 264, 195-205.	4.0	25
215	Influence of accelerating gas flow rate on the particle cohesion in room temperature cold sprayed scattering layer for plastic-based dye-sensitized solar cells. Applied Surface Science, 2014, 288, 416-422.	3.1	9
216	Deposition mechanism of convex YSZ particles and effect of electrolyte/cathode interface structure on cathode performance of solid oxide fuel cell. International Journal of Hydrogen Energy, 2014, 39, 13650-13657.	3.8	9

#	Article	IF	CITATIONS
217	Preparation of Aluminum Coatings by Atmospheric Plasma Spraying and Dry-Ice Blasting and Their Corrosion Behavior. Journal of Thermal Spray Technology, 2013, 22, 1222-1229.	1.6	6
218	Effect of Gas Pressure on Polarization of SOFC Cathode Prepared by Plasma Spray. Journal of Thermal Spray Technology, 2013, 22, 640-645.	1.6	1
219	Characterization of Nonmelted Particles and Molten Splats in Plasma-Sprayed Al2O3 Coatings by a Combination of Scanning Electron Microscopy, X-ray Diffraction Analysis, and Confocal Raman Analysis. Journal of Thermal Spray Technology, 2013, 22, 131-137.	1.6	27
220	Epitaxial Grain Growth During Splat Cooling of Alumina Droplets Produced by Atmospheric Plasma Spraying. Journal of Thermal Spray Technology, 2013, 22, 152-157.	1.6	10
221	Microstructure and Properties of Porous Ni50Cr50-Al2O3 Cermet Support for Solid Oxide Fuel Cells. Journal of Thermal Spray Technology, 2013, 22, 158-165.	1.6	6
222	Development of Particle Interface Bonding in Thermal Spray Coatings: A Review. Journal of Thermal Spray Technology, 2013, 22, 192-206.	1.6	86
223	Effect of Phase Transformation Mechanism on the Microstructure of Cold-sprayed Ni/Al-Al2O3 Composite Coatings during Post-spray Annealing Treatment. Journal of Thermal Spray Technology, 2013, 22, 398-405.	1.6	12
224	Synergistic effects of high temperature and impact compaction on the nano-TiO2 film for the significant improvement of photovoltaic performance of flexible dye-sensitized solar cells. Electrochimica Acta, 2013, 87, 940-947.	2.6	9
225	Scandia-stabilized zirconia electrolyte with improved interlamellar bonding by high-velocity plasma spraying for high performance solid oxide fuel cells. Journal of Power Sources, 2013, 232, 123-131.	4.0	20
226	Modeling Thermal Conductivity of Thermally Sprayed Coatings with Intrasplat Cracks. Journal of Thermal Spray Technology, 2013, 22, 1328-1336.	1.6	45
227	Microstructural and Mechanical Property Evolutions of Plasma-Sprayed YSZ Coating During High-Temperature Exposure: Comparison Study Between 8YSZ and 20YSZ. Journal of Thermal Spray Technology, 2013, 22, 1294-1302.	1.6	71
228	Evolution of Lamellar Interface Cracks During Isothermal Cyclic Test of Plasma-Sprayed 8YSZ Coating with a Columnar-Structured YSZ Interlayer. Journal of Thermal Spray Technology, 2013, 22, 1374-1382.	1.6	64
229	Photovoltaic performance degradation and recovery of the flexible dye-sensitized solar cells by bending and relaxing. Journal of Power Sources, 2013, 226, 173-178.	4.0	17
230	Correlations between milling conditions and iron contamination, microstructure and hardness of mechanically alloyed cubic BN particle reinforced NiCrAl matrix composite powders. Journal of Alloys and Compounds, 2013, 548, 180-187.	2.8	16
231	Critical bonding temperature for the splat bonding formation during plasma spraying of ceramic materials. Surface and Coatings Technology, 2013, 235, 841-847.	2.2	86
232	Effect of TiC addition and high-temperature annealing on the microstructure and electrical conductivity of shrouded-plasma-sprayed FeAl/TiC composites for SOFC support. Journal of Power Sources, 2013, 233, 394-400.	4.0	7
233	Improvement of Adhesion and Cohesion in Plasma-Sprayed Ceramic Coatings by Heterogeneous Modification of Nonbonded Lamellar Interface Using High Strength Adhesive Infiltration. Journal of Thermal Spray Technology, 2013, 22, 36-47.	1.6	39
234	Relationships between feedstock structure, particle parameter, coating deposition, microstructure and properties for thermally sprayed conventional and nanostructured WC–Co. International Journal of Refractory Metals and Hard Materials, 2013, 39, 2-17.	1.7	122

#	Article	IF	CITATIONS
235	Characterization of the microstructure and electrochemical behavior of Sm0.7Sr0.3Co3â^î^´cathode deposited by solution precursor plasma spraying. International Journal of Hydrogen Energy, 2012, 37, 13097-13102.	3.8	17
236	Microstructure, performance and stability of Ni/Al2O3 cermet-supported SOFC operating with coal-based syngas produced using supercritical water. International Journal of Hydrogen Energy, 2012, 37, 13001-13006.	3.8	14
237	Microstructure and polarization of La0.8Sr0.2MnO3 cathode deposited by alcohol solution precursor plasma spraying. International Journal of Hydrogen Energy, 2012, 37, 12879-12885.	3.8	16
238	Dual-scale oxide dispersoids reinforcement of Fe–40at.%Al intermetallic coating for both high hardness and high fracture toughness. Materials Science & Engineering A: Structural Materials: Properties, Microstructure and Processing, 2012, 555, 85-92.	2.6	8
239	Fabrication of Porous Molybdenum by Controlling Spray Particle State. Journal of Thermal Spray Technology, 2012, 21, 1032-1045.	1.6	12
240	Thermal Stability of Microstructure and Hardness of Cold-Sprayed cBN/NiCrAl Nanocomposite Coating. Journal of Thermal Spray Technology, 2012, 21, 578-585.	1.6	41
241	Annealing Effect on the Intermetallic Compound Formation of Cold Sprayed Fe/Al Composite Coating. Journal of Thermal Spray Technology, 2012, 21, 571-577.	1.6	15
242	Isothermal Oxidation Behavior of NiCoCrAlTaY Coating Deposited by High Velocity Air-Fuel Spraying. Journal of Thermal Spray Technology, 2012, 21, 391-399.	1.6	36
243	Formation of Pore Structure and Its Influence on the Mass Transport Property of Vacuum Cold Sprayed TiO2 Coatings Using Strengthened Nanostructured Powder. Journal of Thermal Spray Technology, 2012, 21, 505-513.	1.6	15
244	Effect of Dispersed TiC Content on the Microstructure and Thermal Expansion Behavior of Shrouded-Plasma-Sprayed FeAl/TiC Composite Coatings. Journal of Thermal Spray Technology, 2012, 21, 689-694.	1.6	14
245	A Novel Plasma-Sprayed Durable Thermal Barrier Coating with a Well-Bonded YSZ Interlayer Between Porous YSZ and Bond Coat. Journal of Thermal Spray Technology, 2012, 21, 383-390.	1.6	45
246	Simultaneous strengthening and toughening effects in WC–(nanoWC–Co). Scripta Materialia, 2012, 66, 777-780.	2.6	65
247	Electrical and mechanical properties of nano-structured TiN coatings deposited by vacuum cold spray. Vacuum, 2012, 86, 953-959.	1.6	24
248	Preparation of cBNp/NiCrAl nanostructured composite powders by a step-fashion mechanical alloying process. Powder Technology, 2012, 217, 591-598.	2.1	21
249	Improved Efficiency of over 10% in Dye-Sensitized Solar Cells with a Ruthenium Complex and an Organic Dye Heterogeneously Positioning on a Single TiO ₂ Electrode. Journal of Physical Chemistry C, 2011, 115, 7747-7754.	1.5	141
250	Correlation between microstructure and property of electroless deposited Pt counter electrodes on plastic substrate for dye-sensitized solar cells. Applied Surface Science, 2011, 258, 1377-1384.	3.1	13
251	Effect of annealing on the microstructure and erosion performance of cold-sprayed FeAl intermetallic coatings. Surface and Coatings Technology, 2011, 205, 5502-5509.	2.2	43
252	High strain rate induced localized amorphization in cubic BN/NiCrAl nanocomposite through high velocity impact. Scripta Materialia, 2011, 65, 581-584.	2.6	49

#	Article	IF	CITATIONS
253	Influence of pore structure on ion diffusion property in porous TiO2 coating and photovoltaic performance of dye-sensitized solar cells. Surface and Coatings Technology, 2011, 205, 3205-3210.	2.2	25
254	Characterization of High-Temperature Abrasive Wear of Cold-Sprayed FeAl Intermetallic Compound Coating. Journal of Thermal Spray Technology, 2011, 20, 227-233.	1.6	19
255	Effect of Chemical Compositions and Surface Morphologies of MCrAlY Coating on Its Isothermal Oxidation Behavior. Journal of Thermal Spray Technology, 2011, 20, 121-131.	1.6	37
256	Influence of Deposition Temperature on the Microstructures and Properties of Plasma-Sprayed Al2O3 Coatings. Journal of Thermal Spray Technology, 2011, 20, 160-169.	1.6	44
257	Investigation on the Electrical Properties of Vacuum Cold Sprayed SiC-MoSi2 Coatings at Elevated Temperatures. Journal of Thermal Spray Technology, 2011, 20, 892-897.	1.6	10
258	Interlamellar cracking of thermal barrier coatings with TGOs by non-standard four-point bending tests. Materials Science & Engineering A: Structural Materials: Properties, Microstructure and Processing, 2011, 528, 7641-7647.	2.6	10
259	Multiple strengthening mechanisms of cold-sprayed cBNp/NiCrAl composite coating. Surface and Coatings Technology, 2011, 205, 4808-4813.	2.2	56
260	Influence of gas flow during vacuum cold spraying of nano-porous TiO2 film by using strengthened nanostructured powder on performance of dye-sensitized solar cell. Thin Solid Films, 2011, 519, 4709-4713.	0.8	19
261	Layer-by-Layer Fabrication of Multiple-Dye-Sensitized TiO ₂ Films for Dye-Sensitized Solar Cells by Vacuum Cold Spray. Nanoscience and Nanotechnology Letters, 2011, 3, 483-486.	0.4	5
262	Characterization of cold-sprayed nanostructured Fe-based alloy. Applied Surface Science, 2010, 256, 2193-2198.	3.1	20
263	Influence of TGO Composition on the Thermal Shock Lifetime of Thermal Barrier Coatings with Cold-sprayed MCrAlY Bond Coat. Journal of Thermal Spray Technology, 2010, 19, 168-177.	1.6	98
264	Microstructure and Electrochemical Behavior of a Structured Electrolyte/LSM-Cathode Interface Modified by Flame Spraying for Solid Oxide Fuel Cell Application. Journal of Thermal Spray Technology, 2010, 19, 311-316.	1.6	14
265	Influence of Spray Materials and Their Surface Oxidation on the Critical Velocity in Cold Spraying. Journal of Thermal Spray Technology, 2010, 19, 95-101.	1.6	102
266	Influence of substrate hardness transition on built-up of nanostructured WC–12Co by cold spraying. Applied Surface Science, 2010, 256, 2263-2268.	3.1	50
267	Significant influence of particle surface oxidation on deposition efficiency, interface microstructure and adhesive strength of cold-sprayed copper coatings. Applied Surface Science, 2010, 256, 4953-4958.	3.1	110
268	Performance of a Ni/Al2O3 cermet-supported tubular solid oxide fuel cell operating with biomass-based syngas through supercritical water. International Journal of Hydrogen Energy, 2010, 35, 2904-2908.	3.8	17
269	Effect of composition of NiO/YSZ anode on the polarization characteristics of SOFC fabricated by atmospheric plasma spraying. International Journal of Hydrogen Energy, 2010, 35, 2964-2969.	3.8	40
270	Effect of microstructures on electrochemical behavior of La0.8Sr0.2MnO3 deposited by suspension plasma spraying. International Journal of Hydrogen Energy, 2010, 35, 3152-3158.	3.8	23

#	Article	IF	CITATIONS
271	Fracture toughness measurements of plasma-sprayed thermal barrier coatings using a modified four-point bending method. Surface and Coatings Technology, 2010, 204, 4066-4074.	2.2	76
272	Thermal fatigue behavior of thermal barrier coatings with the MCrAlY bond coats by cold spraying and low-pressure plasma spraying. Surface and Coatings Technology, 2010, 205, 2225-2233.	2.2	84
273	Effect of impact-induced melting on interface microstructure and bonding of cold-sprayed zinc coating. Applied Surface Science, 2010, 257, 1516-1523.	3.1	62
274	Characterization of microstructure and properties of nanostructured Fe-Al/WC intermetallic composite coating deposited by cold spraying. , 2010, , .		0
275	EFFECT OF POWDER STRUCTURE ON MICROSTRUCTURE OF THE OXIDE SCALES FORMED ON COLD-SPRAYED NICRAIY COATINGS. International Journal of Modern Physics B, 2010, 24, 3041-3046.	1.0	1
276	Effect of self-propagating high-temperature combustion synthesis on the deposition of NiTi coating by cold spraying using mechanical alloying Ni/Ti powder. Intermetallics, 2010, 18, 2154-2158.	1.8	23
277	RELATION BETWEEN MICROSTRUCTURE AND THERMAL CONDUCTIVITY OF PLASMA-SPRAYED 8YSZ COATING. International Journal of Modern Physics B, 2010, 24, 3017-3022.	1.0	13
278	Effect of in-flight particle characteristics on the coating properties of atmospheric plasma-sprayed 8mol% Y2O3–ZrO2 electrolyte coating studying by artificial neural networks. Surface and Coatings Technology, 2009, 204, 463-469.	2.2	25
279	Microstructure, oxygen stoichiometry and electrical conductivity of flame-sprayed Sm0.7Sr0.3CoO3â^δ. Journal of Power Sources, 2009, 191, 275-279.	4.0	14
280	Development of a Ni/Al2O3 Cermet-Supported Tubular Solid Oxide Fuel Cell Assembled with Different Functional Layers by Atmospheric Plasma-Spraying. Journal of Thermal Spray Technology, 2009, 18, 83-89.	1.6	18
281	Modeling Aspects of High Velocity Impact of Particles in Cold Spraying by Explicit Finite Element Analysis. Journal of Thermal Spray Technology, 2009, 18, 921-933.	1.6	92
282	Characterization of atmospheric plasma-sprayed La0.8Sr0.2Ga0.8Mg0.2O3 electrolyte. Journal of Power Sources, 2008, 184, 370-374.	4.0	6
283	Cold spraying of Fe/Al powder mixture: Coating characteristics and influence of heat treatment on the phase structure. Applied Surface Science, 2008, 255, 2538-2544.	3.1	86
284	Microstructure development of plasma-sprayed yttria-stabilized zirconia and its effect on electrical conductivity. Solid State Ionics, 2008, 179, 1483-1485.	1.3	7
285	Performance of tubular solid oxide fuel cell assembled with plasma-sprayed Sc2O3–ZrO2 electrolyte. Solid State Ionics, 2008, 179, 1575-1578.	1.3	5
286	Study of oxidation behavior of nanostructured NiCrAlY bond coatings deposited by cold spraying. Surface and Coatings Technology, 2008, 202, 3378-3384.	2.2	104
287	Study on gas permeation behaviour through atmospheric plasma-sprayed yttria stabilized zirconia coating. Surface and Coatings Technology, 2008, 202, 5055-5061.	2.2	41
288	High-Temperature Erosion of HVOF Sprayed Cr3C2-NiCr Coating and Mild Steel for Boiler Tubes. Journal of Thermal Spray Technology, 2008, 17, 782-787.	1.6	58

#	Article	IF	CITATIONS
289	Thermal Failure of Nanostructured Thermal Barrier Coatings with Cold-Sprayed Nanostructured NiCrAlY Bond Coat. Journal of Thermal Spray Technology, 2008, 17, 838-845.	1.6	34
290	Formation of NiAl Intermetallic Compound by Cold Spraying of Ball-Milled Ni/Al Alloy Powder Through Postannealing Treatment. Journal of Thermal Spray Technology, 2008, 17, 715-720.	1.6	45
291	Influence of Powder Porous Structure on the Deposition Behavior of Cold-Sprayed WC-12Co Coatings. Journal of Thermal Spray Technology, 2008, 17, 742-749.	1.6	68
292	Influence of through-lamella grain growth on ionic conductivity of plasma-sprayed yttria-stabilized zirconia as an electrolyte in solid oxide fuel cells. Journal of Power Sources, 2008, 176, 31-38.	4.0	63
293	Microwave sintering of plasma-sprayed yttria stabilized zirconia electrolyte coating. Journal of the European Ceramic Society, 2008, 28, 2529-2538.	2.8	13
294	Low temperature deposition and characterization of TiO2 photocatalytic film through cold spray. Applied Surface Science, 2008, 254, 3979-3982.	3.1	75
295	Cold spraying of Al–Sn binary alloy: Coating characteristics and particle bonding features. Surface and Coatings Technology, 2008, 202, 1681-1687.	2.2	56
296	Effect of in-flight particle velocity on the performance of plasma-sprayed YSZ electrolyte coating for solid oxide fuel cells. Surface and Coatings Technology, 2008, 202, 2654-2660.	2.2	32
297	Influence of substrate hardness on deposition behavior of single porous WC-12Co particle in cold spraying. Surface and Coatings Technology, 2008, 203, 384-390.	2.2	53
298	Effect of heat treatment on the microstructure and property of cold-sprayed nanostructured FeAl/Al2O3 intermetallic composite coating. Vacuum, 2008, 83, 146-152.	1.6	58
299	Influence of Microstructure on the Ionic Conductivity of Plasma-Sprayed Yttria-Stabilized Zirconia Deposits. Journal of the American Ceramic Society, 2008, 91, 3931-3936.	1.9	59
300	Origin of preferential orientation of rutile phase in thermally sprayed TiO2 coatings. Materials Letters, 2008, 62, 1670-1672.	1.3	19
301	Analysis on Rapid Cooling and Epitaxial Solidification of a Plasma-Sprayed Yttria Stabilized Zirconia Splat on a High-Temperature Substrate. , 2007, , 1837.		4
302	Dominant microstructural feature over photocatalytic activity of high velocity oxy-fuel sprayed TiO2 coating. Surface and Coatings Technology, 2007, 202, 63-68.	2.2	13
303	Numerical simulation of deformation behavior of Al particles impacting on Al substrate and effect of surface oxide films on interfacial bonding in cold spraying. Applied Surface Science, 2007, 253, 5084-5091.	3.1	130
304	Effect of heat treatment on the microstructure and microhardness of cold-sprayed tin bronze coating. Applied Surface Science, 2007, 253, 5967-5971.	3.1	29
305	Study on impact fusion at particle interfaces and its effect on coating microstructure in cold spraying. Applied Surface Science, 2007, 254, 517-526.	3.1	103
306	Ionic conductivity and its temperature dependence of atmospheric plasma-sprayed yttria stabilized zirconia electrolyte. Materials Science and Engineering B: Solid-State Materials for Advanced Technology, 2007, 137, 24-30.	1.7	112

#	Article	IF	CITATIONS
307	Erosion Performance of HVOF-Sprayed Cr3C2-NiCr Coatings. Journal of Thermal Spray Technology, 2007, 16, 557-565.	1.6	38
308	Microstructural Characterization of Cold-Sprayed Nanostructured FeAl Intermetallic Compound Coating and its Ball-Milled Feedstock Powders. Journal of Thermal Spray Technology, 2007, 16, 669-676.	1.6	55
309	Fabrication of Nano-TiO2 Coating for Dye-Sensitized Solar Cell by Vacuum Cold Spraying at Room Temperature. Journal of Thermal Spray Technology, 2007, 16, 893-897.	1.6	60
310	Characterization of Nanostructured WC-Co Deposited by Cold Spraying. Journal of Thermal Spray Technology, 2007, 16, 1011-1020.	1.6	97
311	Influence of Annealing on Photocatalytic Performance and Adhesion of Vacuum Cold-Sprayed Nanostructured TiO2 Coating. Journal of Thermal Spray Technology, 2007, 16, 873-880.	1.6	32
312	Influence of Silver Doping on Photocatalytic Activity of Liquid-Flame-Sprayed-Nanostructured TiO2 Coating. Journal of Thermal Spray Technology, 2007, 16, 881-885.	1.6	12
313	Microstructure and Electrical Conductivity of Atmospheric Plasma-Sprayed LSM/YSZ Composite Cathode Materials. Journal of Thermal Spray Technology, 2007, 16, 1005-1010.	1.6	11
314	Preliminary Study of Performance of Dye-Sensitized Solar Cell of Nano-TiO ₂ Coating Deposited by Vacuum Cold Spraying. Materials Transactions, 2006, 47, 1703-1709.	0.4	49
315	Effect of Spray Distance on the Mechanical Properties of Plasma Sprayed Ni-45Cr Coatings. Materials Transactions, 2006, 47, 1643-1648.	0.4	6
316	Characterization of the Microstructure and Electrical Conductivity of Plasma-Sprayed La _{0.5} Sr _{0.5} CoO ₃ Coating. Materials Transactions, 2006, 47, 1654-1657.	0.4	3
317	Deposition Behaviors of Solid Phases in Liquid-Solid Two-Phase Particles in High Velocity Oxy-Fuel Spraying. Materials Transactions, 2006, 47, 1684-1689.	0.4	4
318	Phase Formation during Deposition of TiO ₂ Coatings through High Velocity Oxy-Fuel Spraying. Materials Transactions, 2006, 47, 1690-1696.	0.4	18
319	Optimal design of a convergent-barrel cold spray nozzle by numerical method. Applied Surface Science, 2006, 253, 708-713.	3.1	61
320	Modification of microstructure and electrical conductivity of plasma-sprayed YSZ deposit through post-densification process. Materials Science & Engineering A: Structural Materials: Properties, Microstructure and Processing, 2006, 428, 98-105.	2.6	38
321	Characterization of atmospheric plasma-sprayed Sc2O3–ZrO2 electrolyte coating. Solid State Ionics, 2006, 177, 2149-2153.	1.3	17
322	Examination of factors influencing the bond strength of high velocity oxy-fuel sprayed coatings. Surface and Coatings Technology, 2006, 200, 2923-2928.	2.2	63
323	Microstructural characterization and abrasive wear performance of HVOF sprayed Cr3C2–NiCr coating. Surface and Coatings Technology, 2006, 200, 6749-6757.	2.2	124
324	Tensile deformation behavior of plasma-sprayed Ni–45Cr coatings. Surface and Coatings Technology, 2006, 201, 842-847.	2.2	7

#	Article	IF	CITATIONS
325	Effect of powder structure on microstructure and electrical properties of plasma-sprayed 4.5mol% YSZ coating. Vacuum, 2006, 80, 1261-1265.	1.6	24
326	Relationship between particle erosion and lamellar microstructure for plasma-sprayed alumina coatings. Wear, 2006, 260, 1166-1172.	1.5	97
327	Effect of Annealing Treatment on the Microstructure and Properties of Cold-Sprayed Cu Coating. Journal of Thermal Spray Technology, 2006, 15, 206-211.	1.6	127
328	Examination of the Critical Velocity for Deposition of Particles in Cold Spraying. Journal of Thermal Spray Technology, 2006, 15, 212-222.	1.6	187
329	Characterization of Microstructure of Nano-TiO ₂ Coating Deposited by Vacuum Cold Spraying. Journal of Thermal Spray Technology, 2006, 15, 513-517.	1.6	70
330	Effect of Cu ²⁺ Doping on Photocatalytic Performance of Liquid Flame Sprayed TiO ₂ Coatings. Journal of Thermal Spray Technology, 2006, 15, 582-586.	1.6	9
331	Examination of Substrate Surface Melting-Induced Splashing During Splat Formation in Plasma Spraying. Journal of Thermal Spray Technology, 2006, 15, 717-724.	1.6	33
332	Measurement and Numerical Simulation of Particle Velocity in Cold Spraying. Journal of Thermal Spray Technology, 2006, 15, 559-562.	1.6	26
333	On high velocity impact of micro-sized metallic particles in cold spraying. Applied Surface Science, 2006, 253, 2852-2862.	3.1	155
334	Fracture Toughness of Plasma Spreaged YSZ coatings. Yosetsu Gakkai Ronbunshu/Quarterly Journal of the Japan Welding Society, 2006, 24, 65-69.	0.1	7
335	Influence of substrate roughness on the bonding mechanisms of high velocity oxy-fuel sprayed coatings. Thin Solid Films, 2005, 485, 141-147.	0.8	116
336	Experimental determination of the relationship between flattening degree and Reynolds number for spray molten droplets. Surface and Coatings Technology, 2005, 191, 375-383.	2.2	44
337	Effect of densification processes on the properties of plasma-sprayed YSZ electrolyte coatings for solid oxide fuel cells. Surface and Coatings Technology, 2005, 190, 60-64.	2.2	74
338	Formation of metastable phases in cold-sprayed soft metallic deposit. Surface and Coatings Technology, 2005, 198, 469-473.	2.2	119
339	Effect of spray parameters on the electrical conductivity of plasma-sprayed La1â^'xSrxMnO3 coating for the cathode of SOFCs. Surface and Coatings Technology, 2005, 198, 278-282.	2.2	52
340	Optimal Design of a Novel Cold Spray Gun Nozzle at a Limited Space. Journal of Thermal Spray Technology, 2005, 14, 391-396.	1.6	101
341	Phase Formation of Nano-TiO ₂ Particles during Flame Spraying with Liquid Feedstock. Journal of Thermal Spray Technology, 2005, 14, 480-486.	1.6	32
342	A theoretical model for prediction of deposition efficiency in cold spraying. Thin Solid Films, 2005, 489, 79-85.	0.8	77

#	Article	IF	CITATIONS
343	Effects of annealing treatment on microstructure and photocatalytic performance of nanostructured TiO[sub 2] coatings through flame spraying with liquid feedstocks. Journal of Vacuum Science & Technology an Official Journal of the American Vacuum Society B, Microelectronics Processing and Phenomena, 2004, 22, 2364.	1.6	27
344	Effect of solid carbide particle size on deposition behaviour, microstructure and wear performance of HVOF cermet coatings. Materials Science and Technology, 2004, 20, 1087-1096.	0.8	56
345	Transient Contact Pressure During Flattening of Thermal Spray Droplet and Its Effect on Splat Formation. Journal of Thermal Spray Technology, 2004, 13, 229-238.	1.6	56
346	Dependency of Fracture Toughness of Plasma Sprayed Al ₂ O ₃ Coatings on Lamellar Structure. Journal of Thermal Spray Technology, 2004, 13, 425-431.	1.6	31
347	Effect of specimen geometry on fracture toughness measurement of plasma-sprayed ceramic coatings by the tapered double cantilever beam approach. Vacuum, 2004, 73, 649-654.	1.6	5
348	Performance of YSZ electrolyte layer deposited by atmospheric plasma spraying for cermet-supported tubular SOFC. Vacuum, 2004, 73, 699-703.	1.6	60
349	Effects of spray parameters on the microstructure and property of Al2O3 coatings sprayed by a low power plasma torch with a novel hollow cathode. Thin Solid Films, 2004, 450, 282-289.	0.8	31
350	Microstructure and photocatalytic performance of high velocity oxy-fuel sprayed TiO2 coatings. Thin Solid Films, 2004, 466, 81-85.	0.8	47
351	Evaporated-gas-induced splashing model for splat formation during plasma spraying. Surface and Coatings Technology, 2004, 184, 13-23.	2.2	130
352	Microstructure and property of micro-plasma-sprayed Cu coating. Materials Science & Engineering A: Structural Materials: Properties, Microstructure and Processing, 2004, 379, 92-101.	2.6	22
353	Effect of nano-crystallization of high velocity oxy-fuel-sprayed amorphous NiCrBSi alloy on properties of the coatings. Journal of Vacuum Science and Technology A: Vacuum, Surfaces and Films, 2004, 22, 2000-2004.	0.9	20
354	Microstructure and property of Al2O3 coating microplasma-sprayed using a novel hollow cathode torch. Materials Letters, 2004, 58, 179-183.	1.3	25
355	Title is missing!. Journal of Materials Science Letters, 2003, 22, 1499-1501.	0.5	6
356	Effect of Spray Particle Trajectory on the Measurement Signal of Particle Parameters Based on Thermal Radiation. Journal of Thermal Spray Technology, 2003, 12, 80-94.	1.6	21
357	Effect of sprayed powder particle size on the oxidation behavior of MCrAlY materials during high velocity oxygen-fuel deposition. Surface and Coatings Technology, 2003, 162, 31-41.	2.2	78
358	Deposition characteristics of titanium coating in cold spraying. Surface and Coatings Technology, 2003, 167, 278-283.	2.2	308
359	Measurement of Fracture Toughness of Plasmaâ€5prayed Al ₂ O ₃ Coatings Using a Tapered Double Cantilever Beam Method. Journal of the American Ceramic Society, 2003, 86, 1437-1439.	1.9	24
360	Formation of nanostructured TiO2 by flame spraying with liquid feedstock. Materials Letters, 2003, 57, 2130-2134.	1.3	28

#	Article	IF	CITATIONS
361	Relation Between Microstructure and Properties of HVOF Sprayed Cr3C2-NiCr Cermet Coatings Yosetsu Gakkai Ronbunshu/Quarterly Journal of the Japan Welding Society, 2003, 21, 109-115.	0.1	0
362	Dominant effect of carbide rebounding on the carbon loss during high velocity oxy-fuel spraying of Cr3C2–NiCr. Thin Solid Films, 2002, 419, 137-143.	0.8	86
363	Effect of Particle State on the Adhesive Strength of HVOF Sprayed Metallic Coating. Journal of Thermal Spray Technology, 2002, 11, 523-529.	1.6	50
364	Relationships Between the Microstructure and Properties of Thermally Sprayed Deposits. Journal of Thermal Spray Technology, 2002, 11, 365-374.	1.6	277
365	Effect of types of ceramic materials in aggregated powder on the adhesive strength of high velocity oxy-fuel sprayed cermet coatings. Surface and Coatings Technology, 2001, 145, 113-120.	2.2	33
366	Effect of WC Particle Size on the Abrasive Wear of Thermally Sprayed WC-Co Coatings. Materials and Manufacturing Processes, 1999, 14, 175-184.	2.7	31
367	Effect of Gas Conditions on HVOF Flame and Properties of WC-Co Coatings. Materials and Manufacturing Processes, 1999, 14, 383-395.	2.7	29
368	Effect of Spray Conditions on the Properties of HVOF Sprayed Cr3C2-NiCr Coatings Yosetsu Gakkai Ronbunshu/Quarterly Journal of the Japan Welding Society, 1998, 16, 25-34.	0.1	1
369	The lamellar structure of a detonation gun sprayed Al2O3 coating. Surface and Coatings Technology, 1996, 82, 254-258.	2.2	57
370	Splat Formation and Stacking Behavior of Particles in High Velocity Oxygen-Fuel Spraying of WC-Co Coatings. Nippon Kinzoku Gakkaishi/Journal of the Japan Institute of Metals, 1995, 59, 1130-1135.	0.2	2
371	Quantitative characterization of the structure of plasma-sprayed Al2O3 coating by using copper electroplating. Thin Solid Films, 1991, 201, 241-252.	0.8	158
372	Electrochemical method to evaluate the connected porosity in ceramic coatings. Thin Solid Films, 1988, 156, 315-326.	0.8	49
373	Effect of Powder Size and Volume Fraction of WC on the Microstructure of Laser Cladding WC-NiCrBSi Composite Coatings. Applied Mechanics and Materials, 0, 121-126, 105-109.	0.2	0